

**TWENTYFIFTH EUROPEAN ROTORCRAFT FORUM**

**Paper n° C11**

**HIGH RESOLUTION AERODYNAMIC ANALYSIS OF  
FULL HELICOPTER CONFIGURATIONS**

**SPYROS G. VOUTSINAS, DIMITRIS G. TRIANTOS  
NATIONAL TECHNICAL UNIVERSITY OF ATHENS, GREECE**

**SEPTEMBER 14-16, 1999  
ROME, ITALY**

**ASSOCIAZIONE INDUSTRIE PER L' AEROSPAZIO, I SISTEMI E LA DIFESA  
ASSOCIAZIONE ITALIANA DI AERONAUTICA ED ASTRONAUTICA**

# High Resolution Aerodynamic Analysis of Full Helicopter Configurations

Spyros G. Voutsinas, Dimitris G. Triantos  
National Technical University of Athens, Fluids Section,  
PO Box 64070, 15710 Zografou, Athens, Greece  
tel.: (+)301-7721096, fax: (+)301-7721057, e-mail: aiolos@fluid.mech.ntua.gr

## Abstract

A general framework for cost effective unsteady flow predictions of high resolution around full helicopter configurations is formulated. Starting point is the Helmholtz decomposition of the velocity field in which the vortical part is associated mainly to the wake whereas the potential (irrotational part) is associated to the flow induced by the presence of moving solid boundaries. Reduction of computational cost to a minimum, is accomplished by combining vortex blob approximation of the wakes with boundary integral representations of the potential part. High resolution is achieved by introducing particle-mesh techniques in the wake and sub-grid evaluation of the boundary integral terms. In the present paper the basic part of the methodology is described and numerical results are presented for the limiting case of incompressible and inviscid fluids. Viscous as well as compressibility effects can be introduced by domain decomposition techniques, which are most suitable for taking into account such localised and close to the boundaries flow particularities. These issues are also discussed and some preliminary results are presented.

## 1 INTRODUCTION

The flow problems associated to helicopters and tilt rotor aircrafts constitute a separate category in CFD, because of the dominant role of several independently moving bodies and of strong vortex-to-solid interactions. To complete the picture, one should add the flexibility of the blades, the controls as well as noise which has always been an issue of major concern. This constitutes the complete aeromechanical problem. From an analysis point of view, the ultimate goal is the definition of the suitable theoretical framework within which aerodynamics, aeroelasticity and aeracoustics can be treated in combined form. This perspective has been pointed out by Morino [1] who proposes as general framework the Poincare decomposition. Alternatively one could use the Helmholtz decomposition [2]. The difference of these two theorems is in the rotational part of the flow which in the Helmholtz decomposition is expressed as volume convolution of the vorticity instead of getting it indirectly as in the Poincare theorem [1]. This is a fundamental difference, which forces all of the subsequent analysis. At NTUA the Helmholtz decomposition has been chosen for its direct link to Vortex Methods (VMs) which to our experience can provide powerful computational tools.

The most important issue when considering the complete aeromechanical problem for multi-component aircraft configurations is the computational cost. It is true that current research developments concentrate mostly on grid based CFD methods such as the finite volume and finite element methods. Besides being popular, CFD methods contain in principle all the physics and so their only drawback is the cost. It is expected that computer hardware will be able to overcome the present barriers and that in future, simulations of high resolution will be possible. Meanwhile, fast engineering tools are needed and most probably they will be always used for everyday calculations even if CFD concludes its developments

soon and successfully.

Key point towards cost effective modelling is the proper use of the domain decomposition concept. To this end the flow-field is decomposed into the *near-field* in which the regions close and around the solid boundaries are contained, and the *far-field* which contains the wakes of the different components. The near-field will include any weak shock waves, the boundary layer regions as well as the part of the wakes in contact with the solid boundaries. The rationale for such a decomposition is twofold:

- a) Regarding numerics, there are basically two possibilities: either use a grid based field method or a grid-free Lagrangian vortex method. Field methods are most suitable in handling boundary conditions, flow non-linearities such as shock waves and boundary layers, as well as turbulence closure. Because of the finite extent of the grid, specific inflow conditions are required. They can be set either by extending the grid over a large region and then set undisturbed conditions or by matching with a far-field solution. Extension of the grid is possible only at the expense of high numerical diffusion of free vorticity leading to suppression of the wake induced effects. This leaves matching as the only reasonable choice. On the other hand vortex methods are most suitable in solving vortex convection problems in particular because of their having minimum numerical diffusion. This is due to their inherent ability to concentrate the numerical points only in regions of significant vorticity. However vortex methods have major difficulties in handling viscous boundary conditions and therefore they are inappropriate for the near-field. All of the above, makes the combination of a field method for the near-field with a vortex method in the far-field quite attractive.
- b) The limiting case of incompressible (or subsonic)

and inviscid flows has always played an important role in aerodynamics. From an engineering point of view, such an approximation besides giving a first estimate of loads and of the flow in general, for certain flight conditions, can be even a reasonable compromise. In the past, a lot of work was done on panel methods, recently renamed to Boundary Element Methods (BEMs). Extensions to compressible flows were also realised based on the full-potential equations [3, 4]. Finally, always within the same general context, there exists work on also including viscous effects based on viscous-inviscid strong interaction theory [5, 6, 7]. Common theoretical background for all these works, is the theory of boundary integral equations. The most attractive feature of this theory is that it produces grid-free numerical models which are for this reason, computationally efficient. There is an extensive literature on all aspects of boundary integral methods which is not possible to review here. There is however one important aspect which is usually overlooked. Boundary integral theory constitutes the suitable theoretical tool for defining correct matching procedure between field and vortex methods [8, 9]. There are few works in this connection, all dealing with 2D flows [8, 10]. We are not aware of any work on 3D flows. Possibly this is because all previous work concerned  $\psi - \omega$  field methods which are not extendible to 3D. Also worth noticing is the lack of work on turbulent flows even for 2D flows. This is probably because almost all the work on turbulence closure has been developed for  $\bar{u} - p$  and not  $\psi - \omega$  formulations. In the present paper boundary integral methods are used in defining coupling conditions of  $\bar{u} - p$  field methods with vortex methods.

Based on the above remarks, research work at NTUA was directed towards the development of a concise prediction tool for multi-component configurations with several options for the near-field analysis all sharing the same far-field analysis formulated by grid-free vortex methods. The code was named GENUVP (=GENERAL Unsteady Vortex Particle code) because of its relation to vortex particle or vortex blob approximations. In its current state, the basic version of GENUVP, performs unsteady calculations on multi-component configurations containing one or more rotors [11, 12]. The model also includes rigid body controls and beam like elastic deformations of all blades [13, 14]. Acoustic pressure predictions are performed a posteriori using the aerodynamic results and the Ffowcs-Williams Hawkins equation [15]. The basic version uses boundary element methods (BEM) for approximating the near-field. There are also two more versions still in the process of development. The first uses a home-made Euler finite volume solver (FLUX3D) [16] whereas the second uses an also home-made incompressible Navier Stokes solver equipped

with the Spalart Almaras turbulence model (NS3D) [17]. So far they have been successfully tested the first in the case of the flow over a wing and the second in the case of the flow over a wind turbine blade with massive separation extending from the hub up-to about half of its span. The present paper focuses on the basic version of GENUVP. However indicative results from the other two versions are also presented.

## 2 MATHEMATICAL FORMULATION

### 2.1 Helmholtz decomposition

Consider the unsteady flow of an incompressible and inviscid fluid around a multi-component configuration consisted of  $N_B$  bodies. The bodies are allowed to move independently, a necessary feature for helicopter configurations. Let  $\bar{u}(\bar{x}; t), \bar{x} \in D, t \geq 0$  denote the velocity of the fluid where  $D$  is the flow field. Then according to Helmholtz decomposition theorem,  $\bar{u}$  can be split in two parts: an irrotational and a rotational one. Usually the presence of solid boundaries is included in the irrotational part  $\bar{u}_{solid}$  whereas the wakes are, as expected, included in the rotational part  $\bar{u}_{wake}$ . So,

$$(1) \quad \bar{u}(\bar{x}; t) = \bar{u}_{ext}(\bar{x}; t) + \bar{u}_{solid}(\bar{x}; t) + \bar{u}_{wake}(\bar{x}; t)$$

where  $\bar{u}_{ext}$  denotes a given external field possibly varying in space and time. Green's theorem provides the means to express  $\bar{u}_{solid}$  through surface singularity distributions suggesting the use of BEM's in approximating this term. As for  $\bar{u}_{wake}$ , Biot-Savart law gives,

$$(2) \quad \bar{u}_{wake}(\bar{x}_o; t) = \int_{D_o(t)} \frac{\bar{\omega}(\bar{x}; t) \times (\bar{x}_o - \bar{x})}{4\pi |\bar{x}_o - \bar{x}|^3} dD$$

where  $D_o(t)$  denotes the support of vorticity. From (2), the use of VMs in approximating  $\bar{u}_{wake}$  is straightforward. So decomposition (1) implies as suitable numerical model the combination of BEMs with VMs. The two parts in (1) must be linked to each other through appropriate conditions which will feed  $\bar{u}_{wake}$  with vorticity continuously in time. The exact form of these conditions is discussed in section 2.4.

### 2.2 Boundary Integral Methods and the approximation of $\bar{u}_{solid}$

Boundary Integral Methods are based on Green's theorem and are used in describing the kinematics of fluid flows. Consider a flow field  $D$  extended to infinity and bounded by a closed surface  $S$  containing all solid boundaries together with their wakes. In potential theory, wakes are introduced as vortex sheets, i.e. moving surfaces across which the velocity exhibits a tangential discontinuity whereas pressure remains continuous. In this context the scalar potential  $\phi$  associated to a velocity field  $\bar{u}$ , admits the following representation:

$$(3) \quad \phi(\bar{x}_o) = -\int_S \sigma(\bar{x}) \frac{1}{4\pi r} dS - \int_S \mu(\bar{x}) \frac{\partial}{\partial \nu} \frac{1}{4\pi r} dS$$

where  $r = |\bar{x}_o - \bar{x}|$ ,  $\bar{\nu}$  denotes the unit normal to  $S$  with direction towards  $D$  and  $\sigma, \mu$  denote surface distributions of the jumps of  $\partial\phi/\partial\nu$  (sources) and  $-\phi$  (dipoles) respectively. Differentiating (3) [18],

$$(4) \quad \bar{u}(\bar{x}_o) = \int_S \sigma(\bar{x}) \frac{\bar{r}}{4\pi r^3} dS + \int_S \bar{\gamma}(\bar{x}) \times \frac{\bar{r}}{4\pi r^3} dS$$

where  $\bar{\gamma}$  denotes the surface vorticity defined as  $\bar{\gamma} = \nabla\mu \times \bar{\nu}$ . Since there is only the non-entry boundary condition to satisfy for determining the two unknowns  $\sigma, \mu$ , an artificial interior problem is specified which extends  $\phi$  within  $S$ . Depending on the character of the interior problem chosen, the different formulations can be classified either as *indirect* or as *direct*.

Indirect formulations were first introduced by Hess [19, 18]. In all of the different existing variants, non-lifting bodies are represented by sources, thin lifting surfaces by dipoles and thick wings by a combination of the two. In the last case,  $\mu$  is given specific functional form leaving free only the values of the circulation distribution which is determined by proper use of the Kutta condition along the edge of the wing. For lifting bodies active boundary is also the wake which is introduced as a surface carrying dipoles.

Direct formulations were first introduced by Morino [20] who assumed the volume within  $S$  to be stagnant. So,

$$(5) \quad \phi(\bar{x}_o) = -\int_S \frac{\partial\phi}{\partial\nu}(\bar{x}) \frac{1}{4\pi r} dS + \int_S \phi_s(\bar{x}) \frac{\partial}{\partial\nu} \frac{1}{4\pi r} dS$$

In (5)  $\partial\phi/\partial\nu$  is given directly by the non-entry boundary condition whereas  $\phi_s$  is determined as solution of the integral equation obtained from (5) for  $\bar{x}_o \in S$ . Worth noticing is that Morino's direct potential formulation is the same for lifting and non-lifting bodies. The difference will come from the wake which imposes the existence of a discontinuity for  $\phi_s$  along a line on the surface of any lifting body. For a blade or a wing this line can coincide with the trailing edge and the discontinuity is identical to the circulation distribution also determined by the Kutta condition.

Similarly, the direct counterpart of (4) for the velocity has the form:

$$(6) \quad \bar{u}(\bar{x}_o) = \int_S \bar{\nu}(\bar{x}) \cdot \bar{u}(\bar{x}) \frac{\bar{r}}{4\pi r^3} dS + \int_S (\bar{\nu}(\bar{x}) \times \bar{u}(\bar{x})) \times \frac{\bar{r}}{4\pi r^3} dS$$

in which  $\bar{\nu} \cdot \bar{u}$  is known from the boundary condition leaving as unknown the tangential to  $S$  velocity  $\bar{\nu} \times \bar{u}$ .

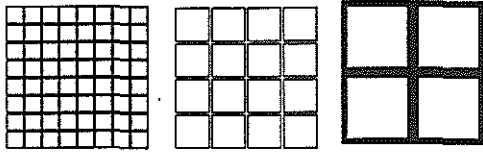
For  $\bar{x}_o \in S$ , the vector product of (6) with  $\bar{\nu}(\bar{x}_o)$  gives two integral equations one for each of the two unknown components of  $\bar{\nu} \times \bar{u}$ . The doubling of the size of the problem is certainly a drawback in using the direct velocity formulation. However the direct calculation of the surface velocity renders this formulation most suitable for coupling BEMs with either integral viscous boundary layer models or with field methods. For lifting bodies, again the wake is introduced as dipole surface, which in the direct velocity formulation is transformed into surface vorticity. More on the wake of lifting bodies and the conditions that quantify the singularity distributions on it will be discussed in subsequent sections.

Regarding the numerics of BEM's there are basically two approximation philosophies: either use dense paneling with piecewise constant singularity distributions [18,19], or introduce high order schemes [21, 22, 23]. Low order schemes are easy to implement but lead to high cost which in fact led some groups to develop high order methods. Besides being more complicated in coding them, they do not match easily with vortex methods, which have zero order accuracy. Also high order panel methods have order mismatch with standard finite volume methods, which use piecewise constant approximations in space. Finally, for lifting bodies special writing of the Kutta condition is needed [24]. For these reasons we decided to proceed with zero order BEM's without disregarding their high cost when paneling gets dense. Fortunately, it is possible to reduce significantly the cost by applying sub-grid techniques.

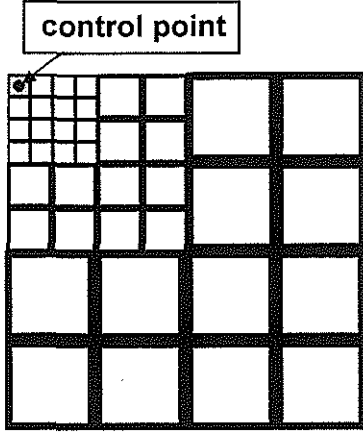
As pointed out early by Hess [19], exact integral evaluations are necessary only when the distance between control point and the panel center is small. In fact when the distance of the evaluation point from the panel gets bigger than 4 times the maximum diagonal of the panel, the integral evaluation can be reduced to a point calculation. Reversing this result, one can expect that the error will be also small if distant panels are grouped into larger ones over which the integrals are evaluated [25]. A strategy to such a grouping has been implemented by introducing a sequence of paneling at different levels of refinement (Fig.1). Calculations start at the lowest level (coarse paneling). Depending on the distance between the panel center and the evaluation point, the calculations will either proceed with the integral evaluation over the large panel or pass to the next and more refined level of paneling. Consider a panel of surface  $S$ , which contains  $n$  panels of the highest level in which the unknown singularity  $X$  is defined. Let  $I_i$  denote the value of the integral evaluated over  $S$  for unitary singularity strength. Then the collective contribution of the  $n$  panels is approximated by:

$$(7) \quad I = \sum_{i=1}^n I_i \frac{S_i}{S} X_i$$

where  $S_i$  denotes the surface area of the  $i$ -th high level panel. Depending on the number of unknowns the final system is either solved directly or iteratively in which



(a) The three levels of paneling



(b) The activation of the different levels

Figure 1 The sub-grid scheme for the evaluation of the boundary integrals

case the matrix need not be stored. Thus panelings of the order of several thousands can be used even on ordinary Workstations.

### 2.3 Vortex Blob Approximations and the management of the wake

Vortex methods were first introduced by Rosenhead back in 1930 [26]. Until early 70's, vortex like methods were applied in aeronautics as part of panel methods to approximate the wake of lifting bodies usually as a set of vortex filaments. Almost simultaneously Basu and Hancock [27] were the first to introduce point vortices in order to predict the unsteady flow around a moving airfoil, whereas Rehbach [28] was the first to formulate a 3D point vortex method for predicting unsteady separated flows over delta wings. At the same period Chorin [29] published his pioneering work on how vortex methods can be applied to simulate the unsteady viscous flow around a cylinder. An excellent review of 3D vortex methods was written by Leonard [30]. In 1982 Beale and Majda publish the first complete work on the mathematical theory of vortex methods [31]. Since then a lot of papers have been published on vortex methods and their applications to all sorts of areas in fluid mechanics which is impossible to review [32]. So the presentation will be restricted to the type of method we implemented in GENUVP.

Vortex methods are defined as one-point quadrature numerical schemes in approximating the volume integral in (2). To this end  $D_\omega(t)$  is decomposed into volume elements  $D_{\omega,j}(t)$ ,  $j \in J(t)$  to each of which a point vortex is defined so that the zero and first moments of  $\bar{\omega}$  are conserved:

Let  $\bar{\Omega}_j(t)$  and  $\bar{Z}_j(t)$  denote the intensity and the position of the  $j$ -th vortex. Then,

$$(8) \quad \bar{\Omega}_j(t) = \int_{D_{\omega,j}} \bar{\omega}(\bar{x};t) dD,$$

$$\bar{\Omega}_j(t) \times \bar{Z}_j(t) = \int_{D_{\omega,j}} \bar{\omega}(\bar{x};t) \times \bar{x} dD$$

so that,

$$(9) \quad \bar{\omega}(\bar{x};t) = \sum_{j \in J(t)} \bar{\Omega}_j(t) \delta(\bar{x} - \bar{Z}_j(t)),$$

$$\bar{u}_{wake}(\bar{x}_o;t) = \sum_{j \in J(t)} \frac{\bar{\Omega}_j(t) \times (\bar{x}_o - \bar{Z}_j(t))}{4\pi |\bar{x}_o - \bar{Z}_j(t)|^3}$$

Because the velocity given by (9b) is highly singular, instead of the Dirac function  $\delta(\cdot)$  in (9a), a smooth approximation is used known as cut-off or regularizing function which can be viewed as localized vorticity distribution function. That is why such vortices are called vortex blobs. Following, Beale and Majda [33], (9b) is written as:

$$(10) \quad \bar{u}_{wake}(\bar{x}_o;t) = \sum_{j \in J(t)} \frac{\bar{\Omega}_j(t) \times \bar{R}_j}{4\pi R_j^3} f_\varepsilon(R_j)$$

where  $\bar{R}_j = \bar{x}_o - \bar{Z}_j$ ,  $\varepsilon$  denotes the cut-off length and  $f_\varepsilon(R_j) = 1 - \exp(-R_j/\varepsilon)^3$ . Usually  $\varepsilon$  is associated to the numerical scales determined by the time step and the grid size of the paneling.

Convection of free vorticity is carried out in Lagrangian description as defined by the corresponding material equations:

$$(11) \quad \frac{d\bar{Z}_j}{dt} = \bar{u}(\bar{Z}_j;t), \quad \frac{d\bar{\Omega}_j}{dt} = (\bar{\Omega}_j \cdot \nabla) \bar{u}(\bar{Z}_j;t) = \bar{D} \cdot \bar{\Omega}_j,$$

where  $\bar{D}$  denotes the deformation tensor. For compressible (barotropic) fluids, (11b) should be modified to include density variations, by substituting  $\bar{\Omega}$  by  $\bar{\Omega}/\rho$ . In this case to each blob, besides the intensity and the position, also the local density is associated. The density is determined by solving the continuity equation, again in Lagrangian form.

Conventional vortex methods involve direct evaluation of the velocity and the deformation at every blob position based on Biot Savart law. This means that for  $N$  vortex blobs a complete time step requires  $N^2$  point-to-point calculations. In engineering applications  $N$  will increase continuously in time and so the computational cost will grow exponentially leading at large times to prohibitive levels. One way of having reasonable cost, is the use of *Particle-Mesh (PM)* techniques [34] which will reduce the cost to  $N \cdot \log N$  operations. The concept is simple: For a large number of blobs,  $\bar{u}$  and  $\bar{D}$  are evaluated at the nodes of a cartesian grid containing  $D_\omega(t)$ . Then local interpolation is used to determine  $\bar{u}$  and  $\bar{D}$  at the exact positions of the blobs. To this end, the vector potential

$\bar{A}$  of  $\bar{u}_{wake}$  is introduced:  $\nabla \times \bar{u}_{wake} = \bar{A}$  and the corresponding Poisson equation:

$$(12) \quad \nabla^2 \bar{A} = -\bar{\omega}, \quad \text{in } D_\omega$$

is solved by means of a Fourier type method implemented by Daube [35]. This choice has been made in order to keep the cost to a minimum. More specifically at every time step the PM calculation procedure involves the following steps:

*The projection step.*

Vorticity is evaluated over a cartesian mesh that includes all vortex blobs, by projecting the intensity of the vortex blobs located within a cell of the mesh to the vertices of the cell:

$$(13) \quad \bar{\omega}_{i,j,k} = \frac{1}{\delta D} \sum_n \bar{\Omega}_n \zeta(\bar{x}_{i,j,k} - \bar{Z}_n)$$

where  $\bar{\omega}_{i,j,k}$  is the nodal vorticity and  $\bar{x}_{i,j,k}$  is the position of node  $(i,j,k)$ ,  $\delta D$  is the volume of the grid cell, and  $\zeta(\cdot)$  is the projection function. The projection function has the form:

$$(14) \quad \zeta(\bar{x}) = w(x) \cdot w(y) \cdot w(z)$$

with  $w(\cdot)$  being defined by one of the following functions,

$$w(x) = \begin{cases} 1 & -h/2 \leq x \leq h/2 \\ 0 & \text{elsewhere} \end{cases}$$

*NGP (nerest grid point) scheme of zero order*

$$w(x) = \begin{cases} 1 - \frac{|x|}{h} & -h/2 \leq x \leq h/2 \\ 0 & \text{elsewhere} \end{cases}$$

*CIC (cloud in cell) scheme of first order*

$$w(x) = \begin{cases} \frac{1}{2}(x^2 + 3hx + 2h^2 + c) / 2h^2, & -3h/2 \leq x \leq -h/2 \\ 1 - (x^2 + c) / h^2, & -h/2 \leq x \leq h/2 \\ \frac{1}{2}(x^2 - 3hx + 2h^2 + c) / 2h^2, & h/2 \leq x \leq 3h/2 \\ 0, & \text{elsewhere} \end{cases}$$

*TSC (triangular shape cloud) scheme of second order*

where  $h$  is the grid step and  $c$  is a free parameter. A fair compromise is the CIC scheme.

*The solution step.*

Equation (12) is discretized with standard central differences leading to three heptadiagonal linear systems,

$$(16) \quad \frac{\bar{A}_{i+1,j,k} - 2\bar{A}_{i,j,k} + \bar{A}_{i-1,j,k}}{\Delta x^2} + \frac{\bar{A}_{i,j+1,k} - 2\bar{A}_{i,j,k} + \bar{A}_{i,j-1,k}}{\Delta y^2} + \frac{\bar{A}_{i,j,k+1} - 2\bar{A}_{i,j,k} + \bar{A}_{i,j,k-1}}{\Delta z^2} = -\bar{\omega}_{i,j,k}$$

The values of  $\bar{A}$  at the boundary nodes of the grid, are provided by point-to-point Biot-Savart calculations:

$$(17) \quad \bar{A}_{i,j,k} = \sum_n \frac{\bar{\Omega}_n}{4\pi |\bar{Z}_n - \bar{x}_{i,j,k}|}$$

To solve (16) first a two-dimensional Fourier transform is performed resulting tri-diagonal linear systems. Then the Thomas algorithm is applied. Finally a reverse two-dimensional Fourier transform follows, which provides the nodal values of  $\bar{A}$ . Once the nodal values of the vector potential are obtained, standard central differences are used to evaluate the velocity  $\nabla \times \bar{A}$  and the deformation vector  $\bar{d} = (\bar{\omega} \nabla) \bar{u}$  at the nodes of the grid.

*The interpolation step.*

The velocity and the deformation of vorticity of each vortex blob are calculated by means of the same procedure used for interpolating the nodal values of vorticity as follows:

$$(18) \quad \bar{u}_n = \sum \bar{u}_{i,j,k} \zeta(\bar{Z}_n - \bar{x}_{i,j,k})$$

$$\frac{d\bar{\Omega}_n}{dt} = \bar{d}_n = \sum \bar{d}_{i,j,k} \zeta(\bar{Z}_n - \bar{x}_{i,j,k})$$

where  $\bar{u}_n$  and  $\bar{d}_n$  denote the velocity and rate of deformation of the  $n$ th vortex blob, whereas  $\bar{u}_{i,j,k}$  and  $\bar{d}_{i,j,k}$  denote the velocity and rate of deformation at grid node  $i,j,k$ . Summation in (18) runs over the neighbouring nodes according to the interpolation scheme.

Accuracy in PM methods is restricted by the cell size. In order to improve the error estimate of PM schemes, Anderson [36] proposed the introduction of local corrections. Because of the  $1/r$  character of the Green function associated to (12), the PM approximation at a point  $\bar{x}_o$ , will be correct as far as concerns distant blobs. For those blobs contained in a *correction area* defined around  $\bar{x}_o$ , a correction  $\Delta \bar{u}$  is added to  $\bar{u}_o$  as calculated by (18a).  $\Delta \bar{u}$  is defined as the velocity directly induced by the blobs contained in the correction area minus their contribution already included in the PM calculation of  $\bar{u}_o$ . The second term is estimated by subtracting their contribution to  $\bar{A}$  at the neighbouring nodes to  $\bar{x}_o$  before (18) is applied. Experience showed that even corrected PM schemes are not sufficiently accurate and therefore they should not be applied to areas of major importance. In GENUVP a mixed scheme has been followed which excludes from the PM calculations areas close to the solid boundaries. In these areas the Biot Savart law is used. For example in the case of helicopters, the PM region starts downstream the tail rotor and extends to infinity.

#### 2.4 The near-to-far field coupling conditions

For an inviscid flow, vorticity can be released into the free flow along specific surface lines such as the

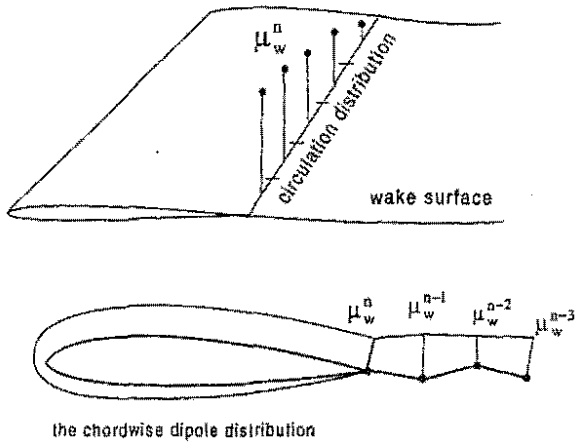


Figure 2 The dipole distribution on the wind and along the wake

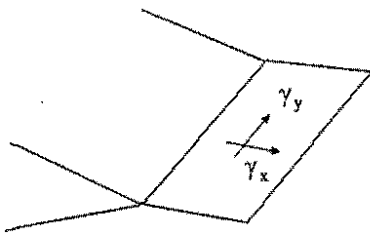


Figure 3 The wake element in the velocity direct formulation

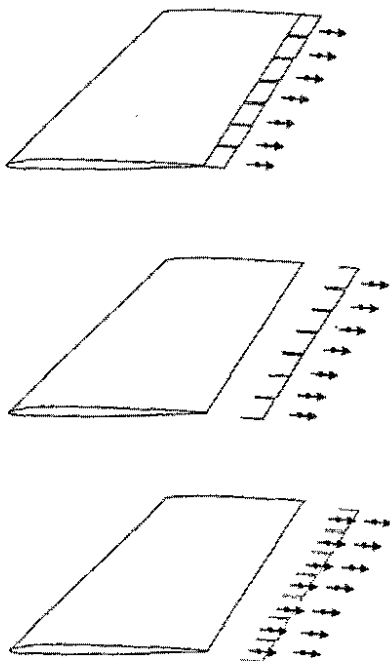


Figure 4 The generation of vortex blobs

trailing edge and the tip of any lifting body as well as a prescribed separation line. This process produces the wake. In most panel approximations, wakes are introduced as vortex sheets, which retain their surface character. Depending on the formulation, the extra unknowns will be either the dipole intensity or the

surface vorticity over the wake surface. In the first case, the dipole intensity at the points of emission is determined by the zero pressure jump condition. Kelvin's theorem then fixes this value for all subsequent time, provided that the wake evolves in a Lagrangian way following the mean flow (See Fig. 2 where superscript  $n$  denotes the time step). In the second case there are two unknowns (Fig.3). Again the zero pressure jump is used but now together with the divergence free condition of the surface vorticity. So the surface vorticity of the part of the wake produced during the current time step is determined. In GENUVP, only the strip of wake generated during the current time step retains its "surface" character (Fig. 4). Subsequently, surface vorticity is treated in particle form through integration. From every panel of the near wake, one or more vortex blobs are generated depending on the desirable length scale. For consistency reasons with the general invariance constraints, the integration should conserve the zero and first moments of vorticity as in (8) except that instead of  $\bar{\omega}$ , the surface vorticity  $\bar{\gamma}$  is introduced. This also holds when the wake is represented by dipoles. In this case it is important to include in the integration also the line vortex elements which appear along the boundaries of the wake panels (Fig. 5).

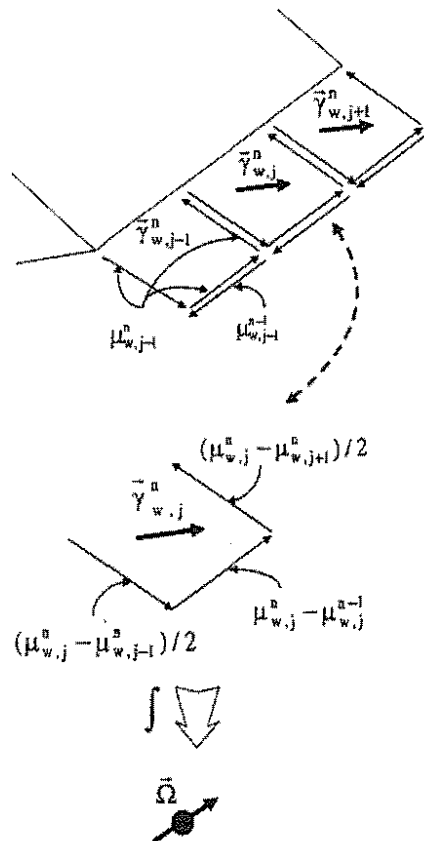


Figure 5 The integration scheme for generating vortex blobs

In a number of applications, it is important to also include separation. A reasonable large-scale approximation is possible by assuming that the principle consequence of separation is the formation of

a pronounced shear layer. For an inviscid approximation, this layer will reduce to a second vortex sheet carrying the corresponding vorticity in condensed form. Provided that the location of separation is known, it is possible to determine the vorticity fed into this second sheet by imposing a zero pressure jump condition. The double wake concept was first introduced for simulating the flow over a delta thin-wing [37]. For thick airfoils Vezza and Galbraith [38] formulated a method of this type based on vorticity representations whereas in [39] the source-dipole method of Basu and Hancock was extended to unsteady separated flows. Also in [39] a 3D thin wing model was formulated for rotating blades in which vorticity is also released from the leading edge at a rate determined by coupling the whole calculation with a section-by-section application of the ONERA stall model. In all these works the location of separation is input externally. In [40] a fully predictive method is proposed for unsteady flows around airfoils, in which separation is predicted by means of a strong viscous-inviscid interaction scheme similar to the one Drela formulated for steady flows [7].

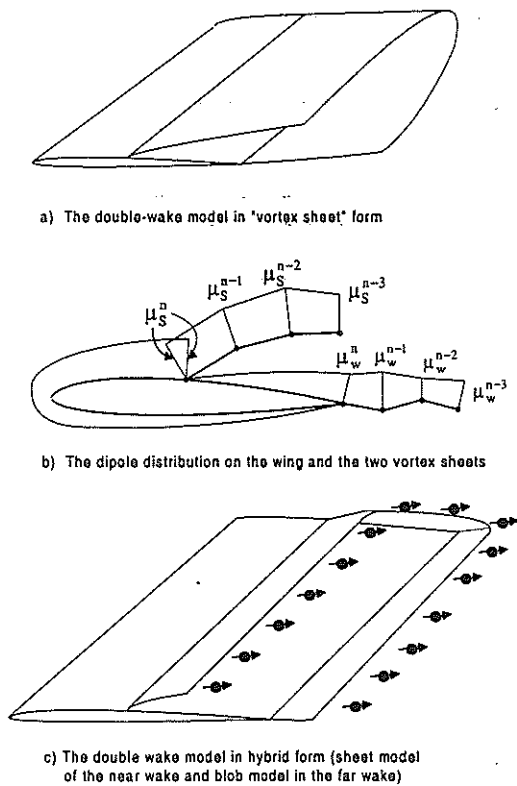


Figure 6 The double-wake scheme in the case of a source-dipole indirect formulation

Figure 6 shows schematically the double wake model in the case of an indirect source-dipole formulation. The bound dipole distribution is given a two-branch form defined by two parameters  $\mu_w, \mu_s$ . Both branches are linear with respect to the surface length. The two wakes will start from the trailing edge and the separation point respectively. Continuity for the dipole distribution is imposed at both emission points.

According to Kelvin's theorem, the values of  $\mu_w, \mu_s$  are fixed to their initial values at all subsequent times. So the dipole distribution over the two wakes is fully defined by the history of the values of  $\mu_w, \mu_s$ . In order to determine the extra unknown  $\mu_s$ , just downstream of separation, the velocity normal to the separation line is set to zero. Similarly a double wake can be also defined for the direct velocity formulation in which case the div free condition for the surface vorticity should be applied also at the separation point.

## 2.5 Extension to aeroelastic analysis

Aeroelastic coupling requires in addition to the structural model, two interfaces. The first will communicate to the aerodynamic part of the calculation the deformations in order to deform the geometry of the bodies as well as the deformation velocities which will be added into the non-entry boundary conditions as external velocity. The second will feed back to the structural model the aerodynamic loads plus their derivatives with respect to the deformation velocities which will determine the aerodynamic damping of the system. In rotor applications, a simple but powerful structural model which is easy to implement, is the beam approximation. Rigid body motions such as rotation, pitch, teeter as well as any other control at the hub, can be directly included. The model implemented in GENUVP was first developed for wind turbine blades [13, 14]. It considers flap and lead-lag bending, torsion and radial tension. The calculation process concerns time domain calculations during which at every step the aerodynamic and structural calculations are performed sequentially.

## 2.6 Extension to viscous flows

The main issue in coupling field with vortex methods is the correct formulation of the coupling conditions. Let  $S$  denote the solid boundary and  $D$  the flow-field, which is decomposed into the near field  $D_{in}$  and the far-field  $D_o$  separated by a closed surface  $S_o$  (Fig 7). In  $D_{in}$  a grid based Navier Stokes solver is used. On  $S$  the non-slip boundary condition is applied whereas on  $S_o$ , the velocity is assumed known. In order to determine the velocity on  $S_o$ , one can use either a purely vortex model or a *boundary projection technique*.

For the purely vortex model, (1) is applied over the entire flowfield with  $\bar{u}_{solid}$  denoting the body velocity and  $\bar{u}_{wake}$  denoting the velocity induced by the entire vorticity field. This part is calculated by the particle-mesh technique. Of course the vorticity used in this calculation, will be that of the previous time step and so the scheme will be explicit. Upon conclusion of every time step vorticity is convected in the form of blobs. Those found outside  $D_{in}$  are retained as vortex blobs belonging to the far field.

In the boundary projection scheme, (1) is applied in  $D_o$  by adding to (6) the extra volume term for the vorticity contained only in the far-field. As explained earlier, expression (6), when applied on  $S_o$ , provides for a given normal velocity distribution



Definition of vorticity boundary values through absorption of incoming blobs

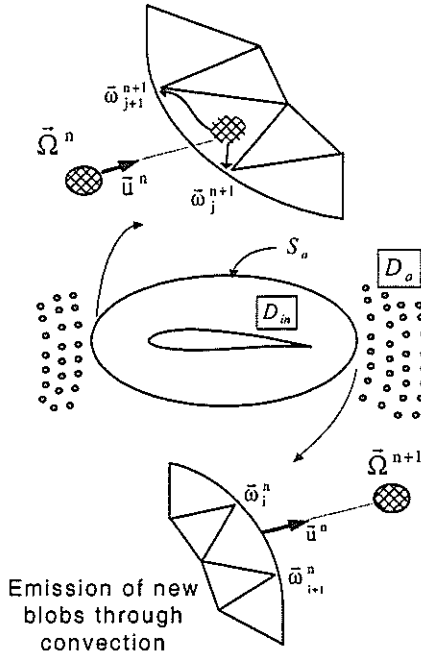


Figure 7 The coupling of a grid-based method with a vortex blob representation of the far field.

$u_n = \bar{u} \cdot \bar{v}$ , the two tangential components  $u_1, u_2$  of  $\bar{u}$  on  $S_o$ . This means that the only unknown is  $u_n$ . Using the definition of  $\bar{\omega}$ ,  $u_n$  can be expressed in terms of  $u_1, u_2$  and  $\bar{\omega}$ . A surface Poisson equation is derived which is integrated over  $S_o$ . So the only unknowns left, are the surface values of  $\bar{\omega}$ . They can be determined by integrating (11b) in a Lagrangian sense as in [10]:

$$(19) \quad \begin{aligned} \bar{\omega}(\bar{x}; t + \delta t) &= \bar{\omega}(\bar{x} - \bar{u}(\bar{x}; t); t) + \\ \delta t \cdot (\bar{\omega}(\bar{x} - \bar{u}(\bar{x}; t); t) \nabla) \bar{u}(\bar{x} - \bar{u}(\bar{x}; t); t) + v.t. \end{aligned}$$

where *v.t.* stands for the viscous terms. At the end of every step vorticity is convected. During this process, vortex particles from the far field can cross  $S_o$  on their way into the near field. In this case they are distributed over the boundary nodes. Also vorticity from the near field can cross  $S_o$  on its way into the wake. In this case the amount of vorticity which is leaving the near field, is transformed into vortex blobs (Fig 7).

### 2.7 Extension to compressible flows

For compressible flows, a volume convolution term for the velocity divergence should be added to (1). For aerodynamic calculations and flows with weak shocks only, this term will be important in the inner region only, provided of course that  $D_{in}$  is sufficiently large. In this case the analysis presented in the previous section can be followed with some modifications. In the purely vortex model, the velocity divergence term should be added in the convection velocity calculations of the vorticity whereas the projection model will remain the same since in  $D_o$  compressibility effects are assumed negligible.

### 3 RESULTS & DISCUSSION

Figure 8 shows an early stage of the computations on a full helicopter configuration using the basic version of GENUVP. All components are included. Wakes are produced by the main and tail rotor blades, the end-plates and the stabilisers.

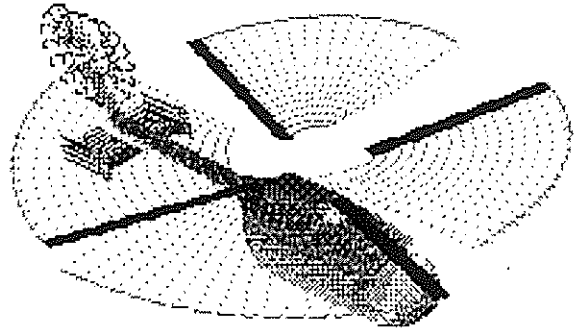


Figure 8 Simulation of full helicopter configuration.

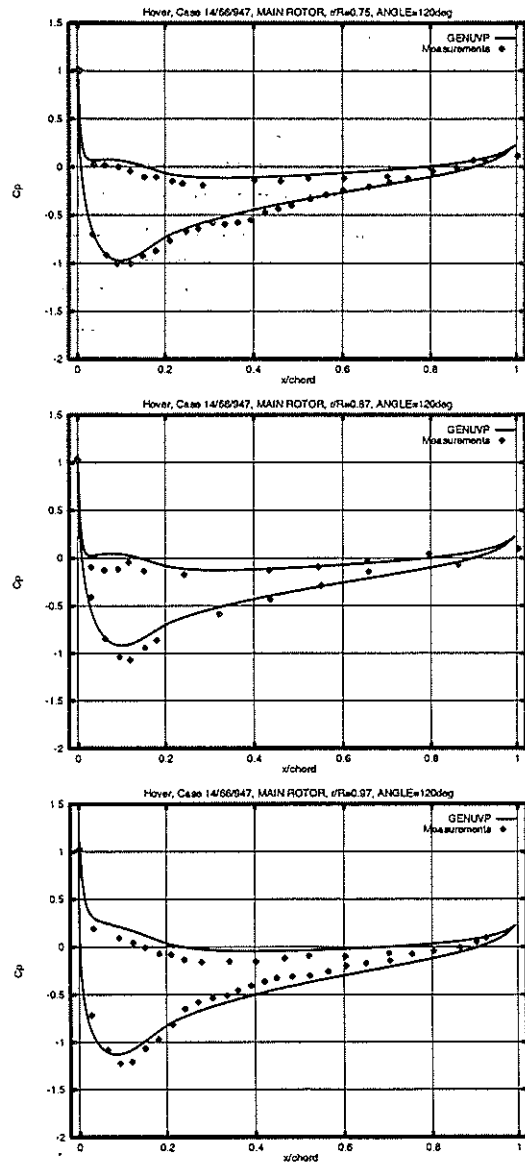


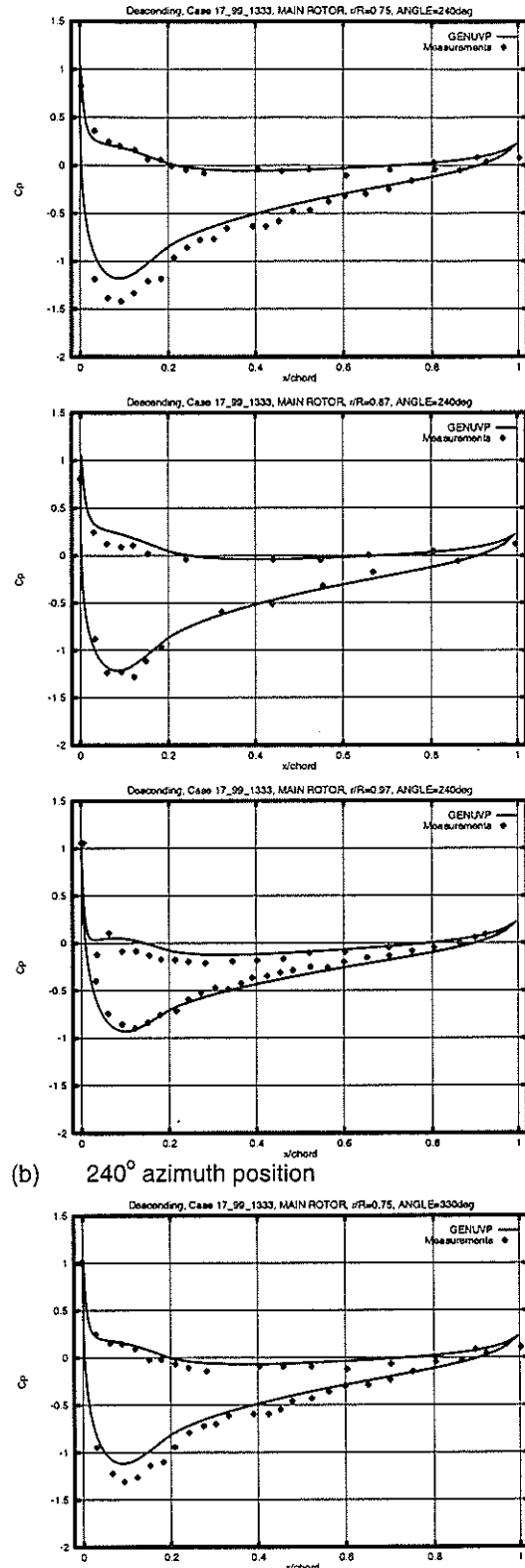
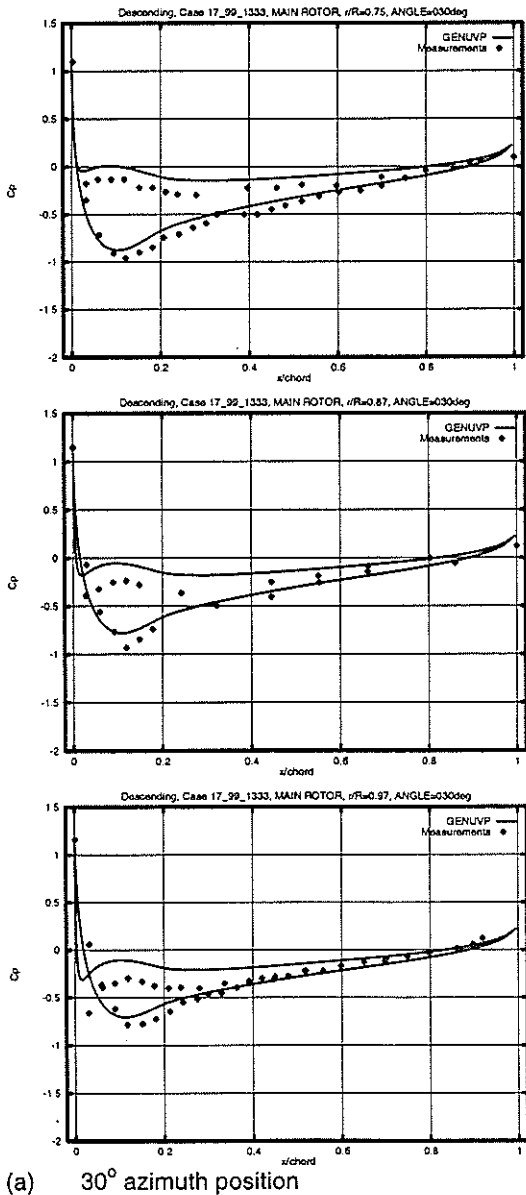
Figure 9 Pressure distributions at 0.75, 0.87 and 0.95 of the BO105 main rotor in low speed hover

Figures 9 and 10 give comparisons of predicted pressure distributions against measurements obtained on the BO105 main rotor blade in the DNW wind tunnel [41]. A three level surface grid of about 10000 panels was used with 90 time steps per revolution. Convergence to a periodic solution was attained after 7 full revolutions. A run of this type for the complete configuration would last 5 days on a single processor Workstation. The first case corresponds to a hover flight situation whereas the second to a descent at  $6^\circ$ , both at  $Ma=0.645$ . Results are presented at 0.75, 0.87 and 0.97 radial stations. In the hover case one azimuth position is given, whereas in the descent case results are shown at azimuth positions  $330^\circ$  and  $30^\circ$  (advancing side) and at  $240^\circ$  (retrieving side). The agreement with measurements is reasonable. There are however differences especially at the  $30^\circ$  azimuth position of the descent case which indicate that the time step as well as the density of the vortex blobs during BVI, need further refinement.

The next test concerns the HART experiment [42]. In Figure 11 the calculated vortex trajectories

are compared to measurements. Although the agreement is quite satisfactory, it is noted that for a complete validation, comparisons should include also velocities. This is a task under way within the future main-tail rotor interaction tests for the BO105 planned to take place in the DNW.

In Figure 12 compressible results are presented for the case of the ONERA M6 wing in steady flow ( $Ma = 0.8395$ ,  $\alpha = 3.06^\circ$ ). In the inner region FLUX3D was used over a grid of  $280 \times 40 \times 27$  extending to 5



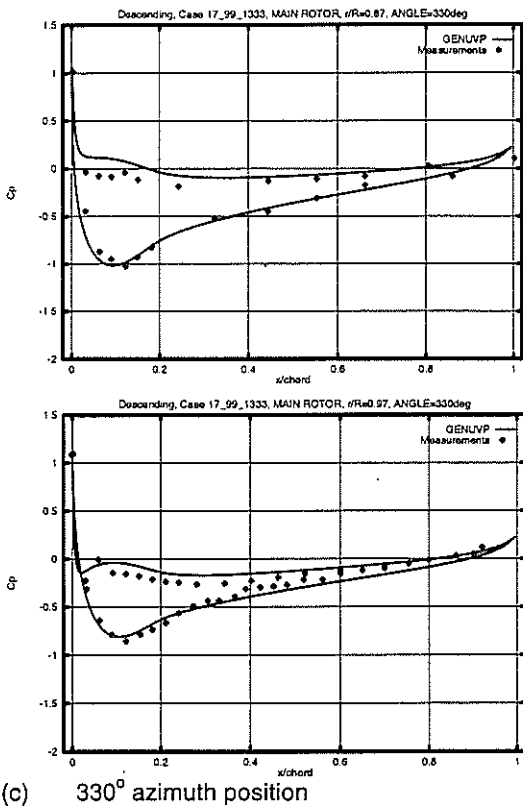


Figure 10 Pressure distributions at 0.75, 0.87 and 0.97 of the BO105 main rotor blade at low speed descent

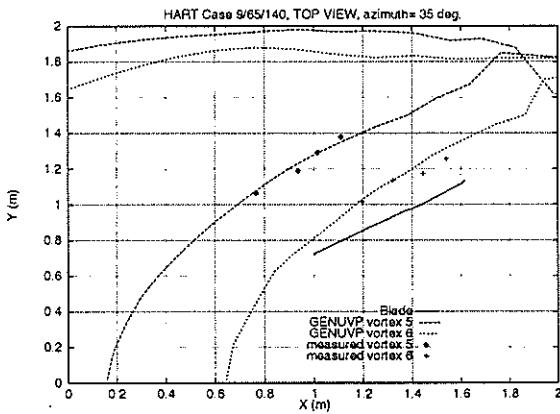
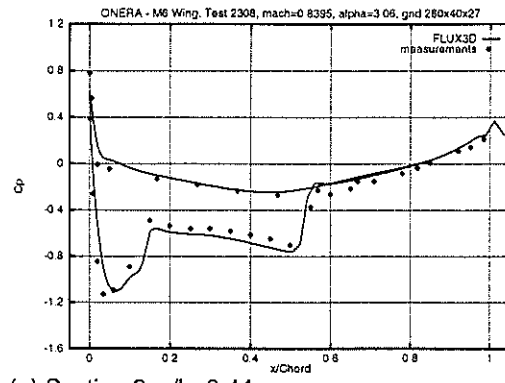


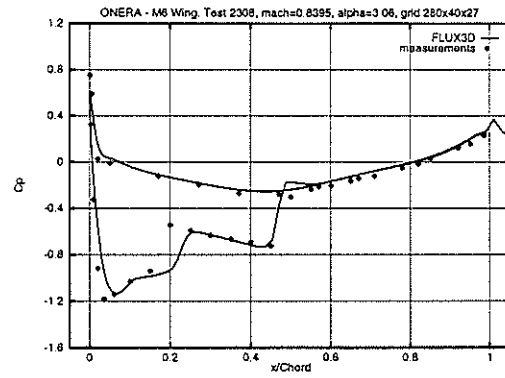
Figure 11 Vortex trajectories from the HART experiment

chords around the wing. In these calculations only the vortex type of coupling was tested. The comparison is quite favourable at least for FLUX3D. As regards the testing of the coupling there is need for a detailed parametric study and therefore the results from this point of view should be regarded as preliminary.

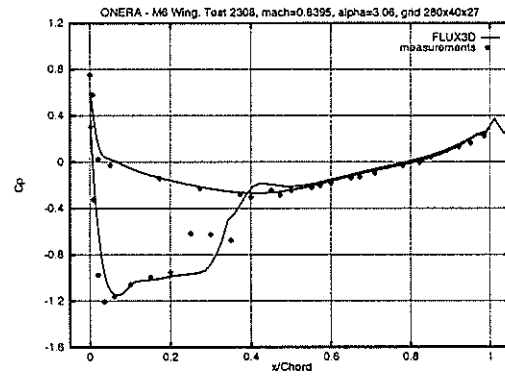
Finally in Figure 13, results from again a steady calculation are presented, this time in the case of an incompressible turbulent flow. The test refers to the case of wind turbine measured by NREL in the USA [43] for which the assumption of incompressibility is certainly valid. The interesting feature in this test is that at mean wind speed of 13m/s, the flow exhibits massive separation over a large extent of the blade. In the inner



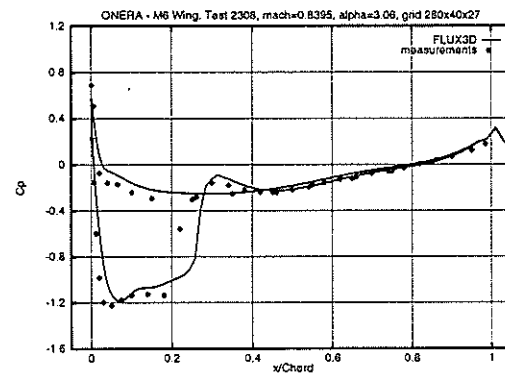
(a) Section 2,  $y/b=0.44$



(b) Section 3,  $y/b=0.65$



(c) Section 4  $y/b=0.8$



(d) Section 6,  $y/b=0.90$

Figure 12 Steady calculations around the ONERA M6 Wing

part covering the region around the blade, NS3D was used. The grid in NS3D is curvilinear and the

arrangement staggered. Also for the pressure, NS3D is based on the SIMPLE algorithm, whereas for turbulence closure the Spalart-Almaras model is used. The coupling with an outer vortex type solution, which again was based on the vortex type model, permits to confine the grid near the blade (again of the order of 5 chord lengths) and yet include the wake induced effects, which to a large extent regulate the flow. For full convergence and for a grid of about  $10^6$  points, the run lasts about 2 days on a single processor of a modern workstation. This is a quite encouraging result since full CFD calculations with multi-block techniques extending the grid both upstream and downstream of the rotor, as reported by NREL, need  $10^7$  points and

several days on high performance computers. As regards the quality of results they are quite satisfactory. There are however differences in the hub region. They could be due to the absence of the hub in the numerical simulations and the artificial boundary condition applied over the first inboard station.

#### 4 CONCLUSIONS

In the present paper Helmholtz decomposition was used in formulating cost effective numerical schemes of high resolution for unsteady flow simulations around multi-component configurations.

First the case of incompressible and inviscid flows was considered, for which Boundary Element and Vortex methods were coupled. High resolution under reasonable cost was accomplished by introducing: (a) Particle-Mesh techniques in the wake, and (b) Sub-grid quadrature for calculating the boundary integrals. Due to its grid-free character, the method is suitable to also include aeroelastic and linear acoustic couplings.

Next, extensions to compressible and/or viscous flows were considered within the context of domain decomposition methods. In this connection two ways for coupling standard CFD methods in the near field with vortex methods in the far field have been proposed, based velocity integral relations of boundary element type.

A series of typical validation tests was presented and predictions were compared to measured data. The overall quality of the predictions is supportive of the promising features of the whole methodology.

#### ACKNOWLEDGEMENTS

The work presented herein, has been funded jointly by the Commission of the European Union under: the HELIFLOW (BE-95-1311) BRITE/EURAM III project, the VISCEL (JOR3-CT98-0208) and COMTER\_ID (JOR3-CT95-0033) JOULE III projects, by the Greek, General Secretariat of Research and Technology under contract EPET#573 and by the Research Committee of the National Technical University of Athens under contracts 66/23 and 66/56.

The authors would like to thank all participants to the HELINOISE and HART projects for providing the measured and technical data used in validating the methods presented herein. From a scientific point of view, the authors thank Prof. L. Morino for all the invaluable discussions and remarks. To a large extent this work has been inspired by his pioneering work.

#### REFERENCES

1. L. Morino (1991) "Helmholtz and Poincare potential-vorticity decompositions for the analysis of unsteady compressible viscous flows", in *Boundary Element Methods in Non-linear Fluid Dynamics 6*, Ed. P.K. Banerjee, L.Morino, Elsevier New York.
2. S.M. Richardson, A.R.H. Cornish (1977) "Solution of three dimensional incompressible flow problems", *J. Fluid Mech.* Vol 82, 309-319
3. O. A. Kandil, E.C. Yates (1986) "Transonic vortex flows past Delta wings: Integral equation approach",

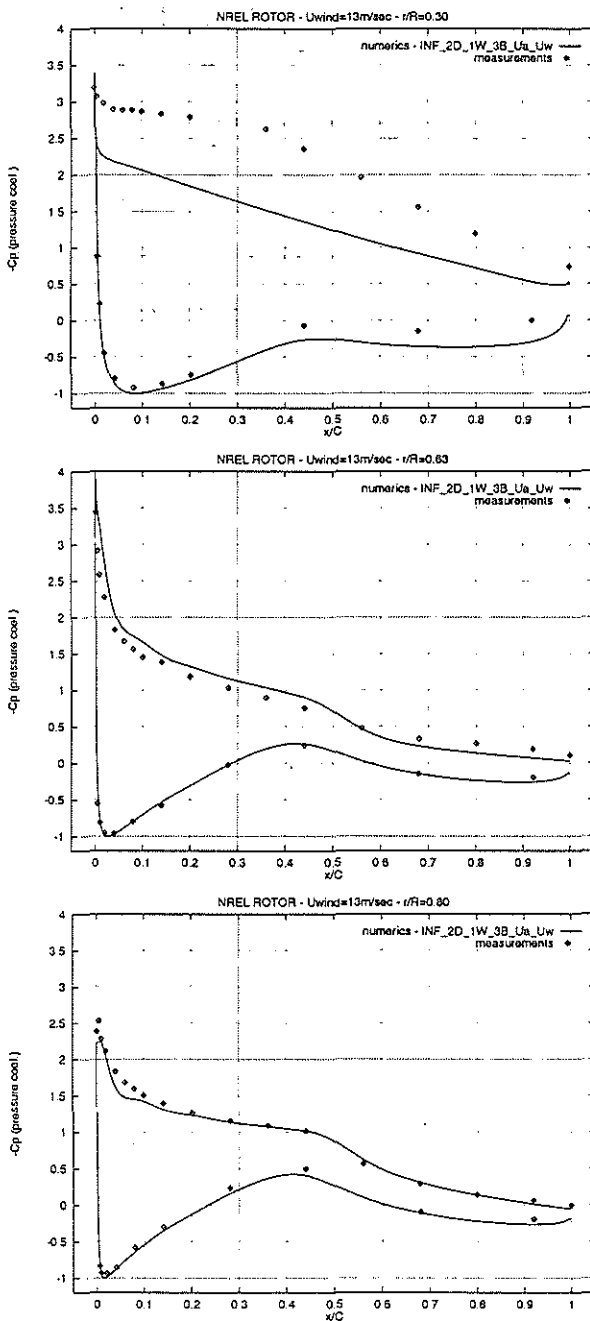


Figure 13 Pressure coefficient distribution for the case of a wind turbine operating at 13m/s wind inflow.

- AIAA J., Vol 24, pp.1729-1736.
4. D. Wehr, L. Zerle, S. Wagner (1996) "Coupling Euler and potential methods for the calculation of helicopter rotors in unsteady forward flight", 22<sup>nd</sup> European Rotorcraft Forum, Brighton UK.
  5. LeBalleur, 1981; "Strong Matching Method for Computing Transonic Viscous Flows including Wakes and Separations. Lifting Airfoils", *Rec. Aerospatiale* no. 1981-3
  6. R.C. Lock. and B.R. Williams (1987) "Viscous-Inviscid Interactions in External Aerodynamics", *Prog. Aerospace Sci.*, vol. 24, pp 51-171
  7. M. Drela (1989) "XFOIL: An Analysis and Design System for Low Reynolds Number Airfoils" Conference on Low Reynolds Number Aerodynamics, University Notre Dame.
  8. J.C. Nedelec, C. Johnson (1973) "On the coupling of integral and finite element methods", *Math. Computation*, Vol 35, 1963-1979
  9. L. Quadrapelle and M. Napolitano (1984) "A method for solving the factorized vorticity-stream function equations by finite elements", *Int. J. Num. Meth. Fluids*, Vol 4, pp. 109-125.
  10. L.J. Guermont, S. Huberson and W.Z. Shen (1993) "Simulation of 2D external viscous flows by means of domain decomposition", *J. Comp. Physics*
  11. S.G. Voutsinas, M.A. Belessis, and K.G. Rados (1995) "Investigation of Yawed Operation of Wind Turbines by means of a Vortex Particle Method", *AGARD-CP-552 Proc. Aerodynamics and Aeroacoustics of Rotorcraft*, Berlin, paper 11
  12. S.G. Voutsinas (1990) "A GENERALIZED Unsteady Vortex Particle method for solving the unsteady flow around multi-component configurations", NTUA Report.
  13. V.A. Riziotis and S.G. Voutsinas (1997) "GAST: A General Aerodynamic and Structural Prediction Tool for Wind Turbines", *Proc. EWEC'97*, Dublin.
  14. S.G. Voutsinas, V.A. Riziotis and D. Mourikis (1996) "Aeroelastic analysis of full wind turbine configurations including controls", NTUA Report
  15. S.G. Voutsinas, D.G. Triantos (1999) "Aeracoustics of full helicopter configurations using vortex particle flow approximations", *Proc. CEAS Forum on Aeracoustics of Rotors and Propellers*, 9-11 June 1999, Rome, Italy.
  16. S.G. Voutsinas, D.G. Triantos (1999) "A coupled finite volume - vortex method for simulating unsteady compressible flows equations", NTUA Report
  17. Y. Perivolaris, V.A. Riziotis, G. Tzabiras and S.G. Voutsinas (1990) "Viscous and aeroelastic effects on wind turbines", NTUA Report
  18. J. L. Hess (1972) "Calculation of potential flow about arbitrary three-dimensional lifting bodies", McDonnell Douglas Rep., MDC J5679-01
  19. J.L. Hess and A.M.O. Smith (1968) "Calculation of Non-Lifting potential flow about arbitrary three-dimensional bodies", McDonnell Douglas Rep. No ES 40622
  20. L. Morino (1974) "A general theory of unsteady compressible potential aerodynamics", NASA CR-2464.
  21. A. Roberts and K. Rundle (1972) "Computation of incompressible flow around bodies and thick wings using the spline-mode system", BAC(CAD) Report Aero Ma 19.
  22. F.T. Johnson, E.N. Tinoco, P. Lu and M.A. Epton (1980) "Three-dimensional flow over wings with leading-edge vortex separation" *AIAA J.*, Vol.18
  23. M. Gennaretti, G. Calcagno, A. Zamboni and L. Morino (1998) "A high order boundary element formulation for potential incompressible aerodynamics", *The Aeronautical Journal*, pp.211-219.
  24. L. Fornasier (1984) "A source equality Kutta condition for panel methods" *AIAA J.* Vol 22, 1167-1169
  25. J.C. Vassberg (1997) "A fast surface panel method capable of solving million-element problems", *AIAA paper 97-0168*
  26. L. Rosenhead (1931) "The formation of vortices from a surface of discontinuity", *Proc. Royal Soc. Ser.A*, 134
  27. B.C. Basu and G.J. Hancock (1978) "The Unsteady Motion of a Two-Dimensional Airfoil in Incompressible, Inviscid Flow", *J. Fluid Mech.*, 87
  28. C. Rehbach (1973) "Calcul d'écoulements autour d'ailes sans épaisseur avec nappes tourbillonnaires évolutives", *Recherche Aerospatiale*, No 2, 53-61.
  29. A. J. Chorin (1973) "Numerical study of slightly viscous flow", *J. Fluid Mech.* Vol. 57.
  30. A. Leonard (1985) "Computing three-dimensional incompressible flows with vortex filaments", *Ann. Rev. Fluid Mech.*, Vol 17, 523-559
  31. J. T. Beale, A. Majda (1982) : "Vortex Methods", *Mathematics of Computation*, Vol. 39.
  32. Y. Gagnon, G-H Cottet, D.G. Drischel, A.F. Ghoniem and E. Meiburg (Ed) (1996) "Vortex flows and related numerical methods II", <http://www.emath.fr/Maths/Proc>.
  33. J. T. Beale, A. Majda (1985) "Higher order accurate vortex methods with explicit velocity kernels", *J. Computational Physics*, Vol. 58.
  34. R. W. Hockney, J. W. Eastwood (1981) "Computer simulation using particles", McGraw-Hill.
  35. O. Daube (1995) "A Fast Poisson solver based on a Fourier Method", personal communication.
  36. C. Anderson (1986) "A method of local corrections for computing the velocity due to a distribution of vortex blobs", *J. Comp. Physics*, Vol 62, 111-123
  37. D. Levin, J. Katz (1981) "Vortex-lattice method for the calculation of the nonsteady separated flow over Delta wings", *J. Aircraft*, Vol. 18
  38. M. Vezza and R.A. Galbraith, R.A. (1985) "An inviscid model of unsteady aerofoil flow with fixed upper surface separation", *J. for Numerical Methods in Fluids*, Vol. 5, pp. 577-592
  39. S.G. Voutsinas and V.A. Riziotis (1996) "Vortex Particle Modeling of Stall on Rotors. Application to Wind Turbines", *Proceedings of the Fluids Engineering Division Summer Meeting, ASME*, San Diego, FED Vol 238, 25-32
  40. S. G. Voutsinas, V. A. Riziotis (1999) "A viscous-inviscid interaction model for dynamic stall simulations on airfoils" *AIAA paper 990038*.
  41. W. R. Splettstoesser, B. Junker, K. J. Schultz, W. Wagner, W. Weitemeyer, A. Protopsaltis, D. Fertis (1993) "The HELINOISE Aeroacoustic Rotor Test in The DNW -Test Documentation and Representative Results-", *DLR Mitteilung* 93-09.
  42. W. R. Splettstoesser, R. Kube, U. Seelhorst, W. Wagner, A. Boutier, F. Micheli, E. Mercker, K. Pengal (1995) "Higher harmonic control aeracoustic rotor test (HART). Test documentation and representative results", *DLR IB 129-95/28*.
  43. J.G. Schepers et al (Ed) (1997) "Final Report of IEA Annex XIV: Field Rotor Aerodynamics", *ECN Report ECN-C-97-027*